Rapid Communications

t-J model on the effective brick-wall lattice for the recently discovered high-temperature superconductor $Ba_2CuO_{3+\delta}$

Zhan Wang,[1] Sen Zhou,[2,3,*] Weiqiang Chen,[4,†] and Fu-Chun Zhang[1,3,‡]

[1]*Kavli Institute for Theoretical Sciences, University of Chinese Academy of Sciences, Beijing 100190, China*

[2]*Institute of Theoretical Physics, Chinese Academy of Sciences, Beijing 100190, China*

[3]*Center for Excellence for Topological Quantum Computation, Chinese Academy of Sciences, Beijing 100190, China*

[4]*Institute for Quantum Science and Engineering and Department of Physics, Southern University of Science and Technology, Shenzhen 518055, China*

(Received 9 February 2020; revised manuscript received 22 April 2020; accepted 28 April 2020; published 18 May 2020)

Layered copper oxides have the highest superconducting transition temperatures at ambient pressure. Its mechanism remains a major challenge in condensed matter physics. The essential physics lying in two-dimensional copper-oxygen layers is well described by a single-band Hubbard model or its strong-coupling limit *t-J* model in a two-dimensional square lattice. The recently discovered high-temperature superconductor $Ba_2CuO_{3+\delta}$ with $\delta \sim 0.2$ has a different crystal structure with a large portion of in-plane oxygen vacancies. We observe that an oxygen vacancy breaks the bond of its two neighboring copper atoms, and propose the ordered vacancies in $Ba_2CuO_{3+\delta}$ lead to an extended *t-J* model on an effective brick-wall lattice. For the nearest-neighbor hopping, the brick-wall model can be mapped onto the *t-J* model on a honeycomb lattice. Our theory explains the superconductivity of $Ba_2CuO_{3+\delta}$ at a high charge carrier density, and predicts a time-reversal symmetry-broken pairing state.

DOI: 10.1103/PhysRevB.101.180509

Introduction. Understanding high T_c copper oxides [1–5] remains a major challenge in condensed matter physics despite intensive studies over the past 30 years. It is generally accepted that the basic physics of high T_c cuprates is on the CuO_2 planes, and the half-filled $d_{x^2-y^2}$ holes of formal Cu^{2+} form a Mott insulator or charge transfer insulator. The chemical doping of the parent compounds introduces additional holes and leads to *d*-wave superconductivity with the highest transition temperatures at ambient pressure. Recently, superconductivity was discovered in $Ba_2CuO_{3+\delta}$ material with $\delta \approx 0.2$, which belongs to a different family of high T_c cuprates [6,7]. The Meissner effect measurement shows that the compound has a transition temperature $T_c = 73$ K, which is much higher than that of a similar structure, the high T_c cuprate $La_{2-x}Ba_xCuO_4$. It is then interesting and important to examine the electronic structure and superconductivity of $Ba_2CuO_{3+\delta}$, which may also shed light on our understanding of high T_c cuprates in general.

$Ba_2CuO_{3+\delta}$ has a compressed octahedron with apical oxygen atoms closer to the central Cu atoms; the Cu-O bond length for apical O is about 1.9 Å, shorter than the Cu-O bond length on the Cu-O plane. This is different from all other known cuprates, where the Cu-O bond along apical O is longer. There are a large number of O vacancies in $Ba_2CuO_{3+\delta}$, which are located on the CuO_2 plane, as neutron data showed [8]. These vacancies are expected to play an important role in the electron structure and possibly superconductivity. First-principles calculations have been reported by Liu *et al.* [9], who considered various possible crystal structures. For $\delta = 0.25$, they have found crystal structures corresponding to lower total energies. There have been a number of proposed theories for its electronic structure and superconductivity. In the usual cuprates, the formal valence of Cu is less than +2.2, corresponding to a hole concentration on the CuO_2 plane of less than 20%. In $Ba_2CuO_{3+\delta}$, the average valence of Cu is $+2(1+\delta)$, corresponding to an average hole concentration of $2\delta \gg 0.2$ for a value of the given $\delta \sim 0.2$. This has led to the proposal of a two-band Hubbard model to describe the compound [10,11]. A large number of O vacancies has led to the proposal of a weakly linked two-chain ladder for the superconductivity [12], whose related physics has been previously examined extensively in the study of Hubbard or *t-J* ladders [13].

In this Rapid Communication, we take the viewpoint that the observed superconductivity in $Ba_2CuO_{3+\delta}$ results from an ordered crystal structure and the O vacancy effectively transforms the original square lattice of CuO_2 to a different lattice. We propose a crystal structure for $Ba_2CuO_{3+\delta}$, where layers of one-dimensional CuO chains and two-dimensional (2D) $CuO_{1.5}$ planes are alternating, as illustrated in Fig. 1(a). We expect the CuO chains to serve as a charge reservoir, in analogy to the CuO chains in $YBa_2Cu_3O_{6+\delta}$ (YBCO), and the $CuO_{1.5}$ planes to contain the essential physics for the superconductivity in $Ba_2CuO_{3+\delta}$. We argue that the effective

*zhousen@itp.ac.cn

†chenwq@sustech.edu.cn

‡fuchun@ucas.ac.cn

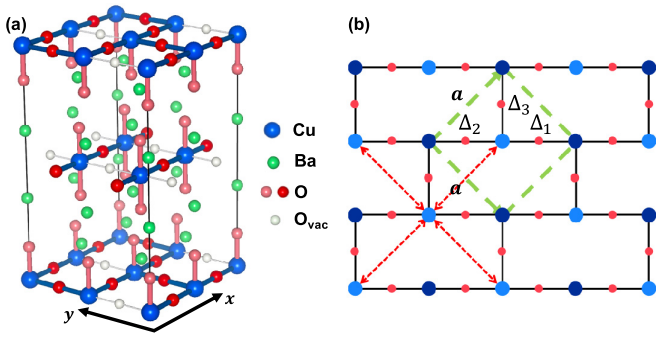

FIG. 1. (a) Proposed crystal structure for $Ba_2CuO_{3.25}$ with an alternating Cu-O chain layer (middle layer) and Cu-$O_{1.5}$ plane (top and bottom layers). The apical O atoms are all occupied. The Cu-$O_{1.5}$ plane forms a brick-wall structure due to the missing O atoms. (b) The brick-wall lattice formed by Cu (light blue for the A sublattice and dark blue for the B sublattice) and O (red) atoms. $\Delta_\alpha, \alpha = 1, 2, 3$ are the superconducting order parameters on the corresponding bonds. The unit cell vectors are depicted as green dashed lines with length a, while the next-nearest neighbors are indicates by the red dashed arrows.

Hamiltonian of a $CuO_{1.5}$ plane is described by a single-band t-t'-J model on an underlying brick-wall lattice, which is shown in Fig. 1(b), with t and t' the nearest-neighbor (NN) and next-nearest-neighbor (NNN) hopping integrals, and J the NN spin-spin coupling of the spin-$\frac{1}{2}$ Cu holes.

We use the renormalized mean-field theory (RMFT) [14] to study the t-t'-J model on the brick-wall lattice. We find that the superconductivity extends to a hole density of as high as 40%, and the maximum of the pairing order parameter appears at a larger hole concentration than the other cuprates due to the shift of the van Hove singularity for the density of states in the brick-wall lattice. The pairing symmetry depends on the value of t'/t and the hole concentration, and may break time-reversal symmetry, which can be tested in a muon spin rotation (μSR) experiment. The effects of bond disorder are also studied, and the superconductivity is expected to survive a weak bond disorder that deviates the structure from a perfect brick-wall lattice.

Our theory appears to be consistent with the available experiments and explains the superconductivity of $Ba_2CuO_{3+\delta}$ with a relatively large hole concentration. We attribute the change of the electronic structure in the planar layer of the compound to the O vacancy, which in turn changes the effective lattice. This may provide another route to study high T_c in the future.

Model and effective lattice. As mentioned above, we consider a crystal structure shown in Fig. 1(a), with alternating layers of CuO chains and $CuO_{1.5}$ planes (x-y plane). The average δ is 0.25 in such a structure. The O vacancies (missing O atoms) in the $CuO_{1.5}$ layer form a square lattice and there are three O atoms around each Cu atom on the plane. The energy of the crystal structure has not been calculated, but should be similar to the one of the lowest-energy crystal structure calculated for $Ba_2CuO_{3.25}$ by Liu *et al.* [9], with the difference being that in the latter case the O vacancies form alternating chains along the x direction. We will focus on the electronic structure of the $CuO_{1.5}$ plane and consider CuO chains to serve as a charge reservoir. While the average of the formal valence of Cu in $Ba_2CuO_{3.25}$ is $Cu^{2.5+}$, the formal valence of the Cu atom on the $CuO_{1.5}$ layer can be significantly smaller because of the compensation from the CuO chains.

For each Cu atom on the $CuO_{1.5}$ plane, there are five nearest-neighbor O atoms including two apical O atoms, two on the x axis, and one on the y axis. The possible antibonding Cu-3d orbitals here are $3d_{3z^2-r^2}$ or $3d_{z^2-x^2}$, whose relative energies depend on the difference or ratio of the bond lengths between the short apical Cu-O bond and the in-plane Cu-O bond. Here, we assume orbital $3d_{3z^2-r^2}$ to have a higher energy, which is consistent with a density-functional calculation for proper parameters [15]. Then the lowest energy of the atomic $3d$ hole state is $d_{3z^2-r^2}$, which replaces $3d_{x^2-y^2}$ in other cuprates as the relevant orbital. Considering Cu-$3d^{10}$ and O-$2p^6$ as the vacuum configuration, the formal Cu^{2+} thus has one hole primarily on Cu-$3d_{3z^2-r^2}$. Because of the large repulsive interaction U for two holes on the same Cu site, the ground state at the half-filling, namely one hole per Cu atom in average, will be a Mott insulator, similar to that of La_2CuO_4.

We next consider additional holes for the half-filled case. As a soft-x-ray absorption experiment [6] showed, the additional hole largely goes to the O-$2p$ orbitals, which implies that the formal Cu^{3+} has one hole on Cu-$3d_{3z^2-r^2}$ and the other on O-$2p$. We expect them to form a spin singlet, similar to the Zhang-Rice spin singlet [16] formed in other cuprates, and move through the lattice as a charge carrier.

Since the hopping of the hole between the two neighboring Cu atoms is essentially mediated by the oxygen $2p$ orbitals in between, it is strongly suppressed if the oxygen between the two Cu atoms is missing. Therefore, the nearest-neighbor Cu-Cu bond may be effectively removed from the lattice if the O atom between them is missing. This leads to an effective brick-wall lattice as shown in Fig. 1(b).

As we discussed above, the physics in $Ba_2CuO_{3+\delta}$ may be similar to that in other cuprates and we may consider the material as a doped Mott insulator within a single orbital model, although the relevant Cu-3d orbital and the underlying lattice due to the missing O ions will be different from the other cuprates. The low-energy physics of $Ba_2CuO_{3.25}$ is thus described by a two-dimensional t-J model on a brick-wall lattice,

$$\mathcal{H} = -\sum_{ij}(t_{ij}P_G c^\dagger_{i\sigma}c_{j\sigma}P_G + \text{H.c.}) + J\sum_{\langle ij\rangle}\mathbf{S}_i\cdot\mathbf{S}_j, \quad (1)$$

where $c_{i\sigma}$ and $c^\dagger_{i\sigma}$ are the annihilation and creation operators of electrons with spin σ at site i, respectively, t_{ij} is the hopping integral of electrons between site i and j, P_G is the Gutzwiller projection operator to project out doubly occupied electron states on the Cu sites, and $\langle ij\rangle$ means NN pairs of i and j. Repeated spin indices are summed. As we analyzed above, the dominant orbital is $3d_{3z^2-r^2}$, thus the hopping integrals are isotropic along the x and y axes. We consider only the case with NN and NNN hoppings, whose hopping integrals are $t_{nn} = t$ and $t_{nnn} = t'$, respectively.

Mean-field results. As shown in Fig. 1(b), the superconducting order parameters of the brick-wall lattice are denoted by Δ_α with $\alpha = 1, 2, 3$. Usually, the symmetry of a system

TABLE I. Character table of group $\mathcal{D}_2$.

Reps	e	$C_2(z)$	σ_x	σ_y
A	$+1$	$+1$	$+1$	$+1$
B_1	$+1$	$+1$	-1	-1
B_2	$+1$	-1	$+1$	-1
B_3	$+1$	-1	-1	$+1$

will impose some constraints on the order parameters. The point group symmetry of the brick-wall lattice is $\mathcal{D}_2$, which has four irreducible representations as listed in Table I. Since we are only interested in spin singlet pairing, only the A and B_1 representations are relevant. For the A representation, we have real pairings with $\Delta_1 = \Delta_2$. For the B_1 representation (which will be denoted as B hereafter), we have real pairings with $\Delta_1 = -\Delta_2$, $\Delta_3 = 0$.

$t' = 0$ is a special case, where the Hamiltonian has a higher symmetry than the lattice, the D_6 symmetry. This can be understood as follows. The brick-wall lattice can be treated as a squeezed honeycomb lattice. If one considers only the NN coupling, the model can be mapped onto a t-J model with the NN hopping on a honeycomb lattice, and has a D_6 symmetry (see the details in the Supplemental Material [17]). Previous studies [18–23] on the t-J model on a honeycomb lattice have suggested a $d + id$-wave topological superconducting phase which corresponds to a two-dimensional representation of the D_6 group. Although the D_6 symmetry is reduced to D_2 as one turns on the NNN hopping, it is possible that the pairing symmetry may still be $d + id$, or more precisely, $A + iB$ in the D_2 case, where the 2D representation reduces to $A \oplus B$, for small t'. In the following calculations, we will take the $A + iB$ ansatz $\Delta_1 = \Delta_2^* = \Delta_{xA} + i\Delta_{xB}$ and $\Delta_3 = \Delta_y$, where Δ_{xA}, Δ_{xB}, and Δ_y are all real, as shown in Fig. 2(a). Δ_{xA} and Δ_{xB} track the contribution from A and B, respectively, a case with finite Δ_{xA} and vanished Δ_{xB} corresponds to a pure A phase, while a case with finite Δ_{xB} and $\Delta_{xA} = \Delta_y = 0$ corresponds to a pure B phase.

Then we solve the superconducting order parameters with the standard renormalized mean-field theory approach (see the details in the Supplemental Material [17]), and the results for $t' = 0$, $t' = 0.1$, and $t' = -0.1$ are depicted in Figs. 2(b)–2(d), respectively. The result for $t' = 0$ shows a time-reversal symmetry-breaking $A + iB$-wave ($d + id$-wave) phase in the large doping regime, which is consistent with the previous studies on a honeycomb lattice. The optimal doping of the superconducting dome corresponds to the van Hove singularities as shown in the inset of Fig. 2(b). For small but finite $t' = \pm 0.1t$, we still have the $A + iB$ phase at low doping ($p < 0.15$). But with increasing doping, the $A + iB$ phase becomes energetically unfavorable and is replaced by a pure B phase (for $t' = 0.1t$) or a pure A phase (for $t' = -0.1t$) [see Figs. 2(e) and 2(f)]. In each phase, we find that the doping with a maximum superconducting order parameter corresponds to the peak in the density of states, i.e., the van Hove singularities.

We also perform the calculations for various dopings and t', and the resultant phase diagram is shown in Fig. 3. One can find a robust $A + iB$ phase in a rather large

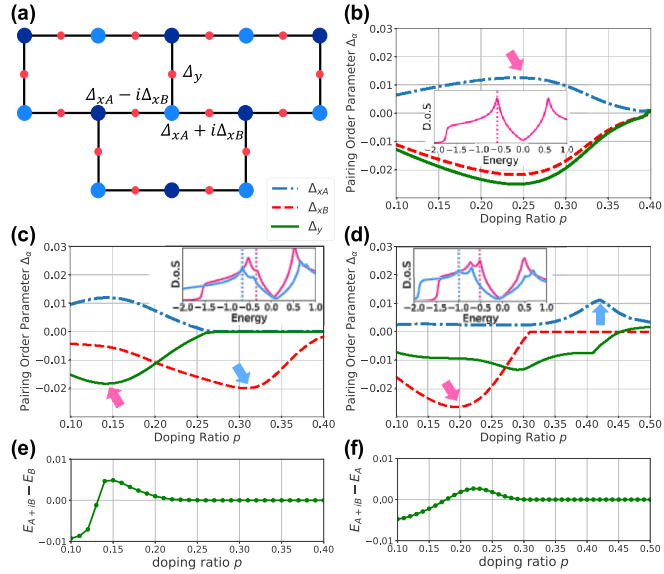

FIG. 2. The RMFT result of the $A + iB$ phase. Δ_{xA} (Δ_{xB}) is used to indicate the contribution from the A (B) representation, respectively. The pairing order parameters on three distinct bonds are indicated in (a). Δ_{xA}, Δ_{xB}, and Δ_y obtained from the RMFT for (b) $t' = 0$, (c) $t'/t = 0.1$, and (d) $t'/t = -0.1$ with $J/t = 0.4$ for all cases. The insets in (b)–(d) are the density of states (DOS) and the corresponding Fermi energy at the optimal dopings marked by the arrows. The energy difference between the $A + iB$ phase and the pure B (A) phase for parameters of (c) [(d)] are shown in (e) [(f)], respectively.

parameter regime and a phase transition from the $A + iB$ phase to A phase in the $t' < 0$ region and a transition from the $A + iB$ to B phase in the $t' > 0$ region. The different behavior between positive and negative t' can be understood

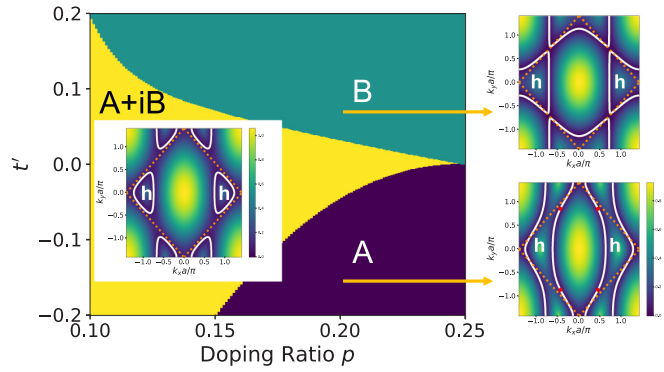

FIG. 3. Phase diagram of different pairing symmetries obtained from RMFT calculation. The yellow, green, and purple regions corresponding to the $A + iB$, pure B, and pure A phases, respectively. We also depict the typical Fermi-surface topology and quasiparticle gap in the Brillouin zone for each phase ($t' = 0$ and $p = 0.15$ for the $A + iB$ phase, $t' = 0.1t$ and $p = 0.31$ for the B phase, and $t' = -0.1$ and $p = 0.36$ for the A phase). The orange dotted lines are the boundary of the reduced Brillouin zone, while the symbol h indicates the region occupied by holes. The $A + iB$ and B phases are gapped, while the A phase is gapless with its nodes depicted as red spots in the figure.

from the Fermi-surface geometry. In Fig. 3, we depict the typical Fermi surface for each phase. In the large doping regime, the underlying Fermi surface for $t' > 0$ has very good nesting along the k_x direction that favors a one-dimensional instability, while the Fermi surface for $t' < 0$ does not have such a nesting and favors a two-dimensional instability. On the other hand, the superconducting pairing in the B phase is one dimensional (because $\Delta_y = 0$), while the pairing in the A phase is more two dimensional. Thus one has the B phase at $t' > 0$ and A phase at $t' < 0$ in the large doping regime.

As we analyzed above, the $A + iB$ phase at $t' = 0$ corresponds to $d + id$ superconductivity, thus the $A + iB$ phase should also be a topological superconducting phase. To confirm that, we calculated the Chern number $\nu_{\rm Ch}$ associated with each phase. We find that the $A + iB$ phase has a Chern number $\nu_{\rm Ch} = 4$, while the pure A and B phase is topologically trivial and has a Chern number $\nu_{\rm Ch} = 0$. Thus, the phase transition between them is indeed a topological phase transition associated with a gap closing behavior.

Effects of bond disorder. It is natural to expect the existence of bond disorder in a system that deviates from the structure of a perfect brick-wall lattice, and its effects on the superconductivity need to be investigated.

We start with an $N = 32 \times 32$ brick-wall lattice of periodic boundary condition, in which there are $3N/2$ NN bonds with a nonzero hopping integral t and superexchange J, forming the structure depicted in Fig. 1(b). Note that, as compared with the square lattice, there are $N/2$ NN bonds missing in the brick-wall lattice. To introduce bond disorder, $N_{\rm dis}$ NN bonds are redistributed randomly. Explicitly, we take out $N_{\rm dis}$ bonds randomly from the $3N/2$ NN bonds of the brick-wall lattice and then distribute them randomly to the place of $N/2$ previously missing bonds. Clearly, $N_{\rm dis}$ takes an integer value between 0 and $N/2$, and the strength of the bond disorder is measured by a value of $\eta = 2N_{\rm dis}/N$. At a given η, we generate 20 disorder realizations and obtain the ground state of each realization self-consistently. We stay with $t' = 0$ and doping concentration $\rho = 0.25$ where the superconducting brick-wall lattice is in the $A + iB$ phase. The average renormalized pairing of each disorder realization, $\tilde{\Delta} = \frac{2}{3N}\sum_{\langle i,j\rangle} g^t_{ij}|\Delta_{ij}|$, at zero temperature is plotted in Fig. 4(a) as crosses at various disorder strengths η, with the solid line representing their ensemble averages. The ensemble-averaged $\tilde{\Delta}$ decreases linearly as the disorder strength η increases, and saturates to a nonzero minimum value at $\eta \simeq 0.09$. We thus expect the superconductivity on the perfect brick-wall lattice to survive weak bond disorders. To estimate the effects of bond disorder on the superconducting transition temperature T_c, the temperature dependence of $\tilde{\Delta}$ is plotted in Fig. 4(b) for $\eta \simeq 0.038$ and $\eta \simeq 0.078$, with the result in the absence of disorder ($\eta = 0$) also shown for comparison. Clearly, the suppression of the mean-field critical temperature by bond disorder is much weaker than the suppression of the ensemble-averaged $\tilde{\Delta}$ at zero temperature.

Figure 5(a) shows the evolution of the DOS, ensemble averaged over 20 disorder realizations, as a function of the bond disorder strength η, with the DOS of each disorder realization provided in Figs. 5(b) and 5(c) for, respectively, $N_{\rm dis} = 1$ and $N_{\rm dis} = 10$. Clearly, the redistribution of a single NN bond in the brick-wall lattice can already produce some in-gap states. This implies that the effect of bond disorder is more than providing a scattering potential. Furthermore, the full superconducting gap in the clean $A + iB$ phase closes at roughly $N_{\rm dis} = 8$, as is evident by a nonzero DOS at the Fermi energy. It would be interesting to study the topology of the superconducting state with bond disorder.

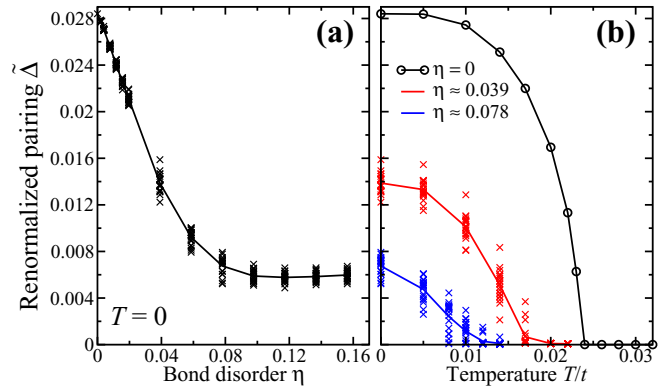

FIG. 4. (a) Ensemble-averaged renormalized pairing $\tilde{\Delta}$ as a function of bond disorder strength η at zero temperature. (b) Temperature dependence of the ensemble-averaged $\tilde{\Delta}$ at bond disorders $\eta = 0$, $\eta \simeq 0.039$, and $\eta \simeq 0.078$. Crosses represent the data of each disorder realization.

Conclusion. In summary, we have proposed an effective brick-wall t-t'-J model for a recently discovered high T_c superconductor. By using renormalized mean-field theory, we have demonstrated that the superconductivity extends to a very large hole concentration, and the pairing order parameter is peaked at a larger hole concentration. The pairing symmetry can be complex and breaks time-reversal invariance, similar to

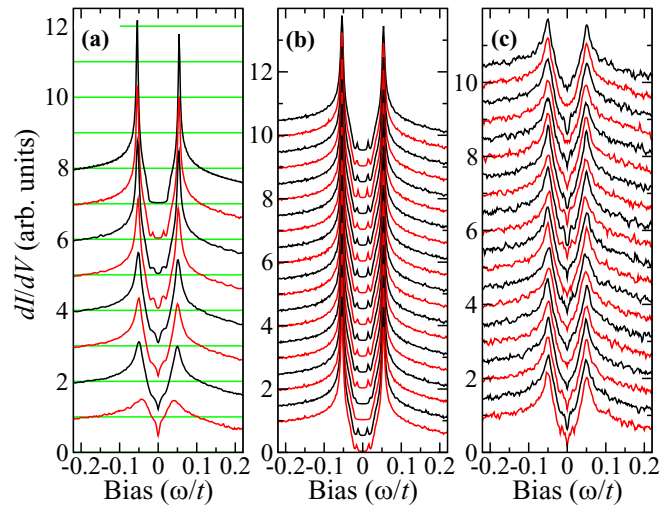

FIG. 5. (a) Evolution of the ensemble-averaged DOS as a function of the bond disorder strength $\eta = 2N_{\rm dis}/N$ with, from top to bottom, $N_{\rm dis} = 0$, 1, 2, 4, 6, 8, 10, and 20. (b) The individual DOS of 20 disorder realizations with $N_{\rm dis} = 1$. (c) Same as (b) but for $N_{\rm dis} = 10$. All curves are offset vertically for clarity.

the superconductivity theoretically studied for the t-J model on the honeycomb lattice. The broken time-reversal symmetry and the chiral edge states originating from its topological nature may be observed with various techniques, such as μSR, Kerr effect, superconducting quantum interference device (SQUID), etc. We note that the Hubbard model on a square lattice has recently been studied using more sophisticated numerical methods. Our study, based on renormalized mean-field theory on the brick-wall lattice, may be viewed as a starting point for these more advanced numerical methods. Our mean-field result on the bond disorder effect suggests a relatively weaker reduction to the superconductivity transition temperature.

Acknowledgments. We wish to thank C. Q. Jin and Q. Z. Huang for many useful discussions on the experimental results, and Congcong Le for the density-functional theory calculations to estimate the energy of the local electronic configurations. We would also like to thank J. P. Hu, Z. Q. Wang, and K. Jiang for many stimulating discussions. This work is in part supported by the National Natural Science Foundation of China (Grants No. 11674151, No. 11847612, No. 11974362, and No. 11674278), National Key Research and Development Program of China (Grant No. 2016YFA0300300), the Strategic Priority Research Program of CAS (Grant No. XDB28000000), and Beijing Municipal Science and Technology Commission (Grant No. Z181100004218001).

[1] B. Keimer, S. A. Kivelson, M. R. Norman, S. Uchida, and J. Zaanen, Nature (London) **518**, 179 (2015).
[2] P. W. Anderson, P. A. Lee, M. Randeria, T. M. Rice, N. Trivedi, and F. C. Zhang, J. Phys.: Condens. Matter **16**, R755 (2004).
[3] T. M. Rice, K.-Y. Yang, and F. C. Zhang, Rep. Prog. Phys. **75**, 16502 (2011).
[4] J. G. Bednorz and K. A. Müller, Z. Phys. B: Condens. Matter **64**, 189 (1986).
[5] P. A. Lee, N. Nagaosa, and X.-G. Wen, Rev. Mod. Phys. **78**, 17 (2006).
[6] W. M. Li, J. F. Zhao, L. P. Cao, Z. Hu, Q. Z. Huang, X. C. Wang, Y. Liu, G. Q. Zhao, J. Zhang, Q. Q. Liu, R. Z. Yu, Y. W. Long, H. Wu, H. J. Lin, C. T. Chen, Z. Li, Z. Z. Gong, Z. Guguchia, J. S. Kim, G. R. Stewart *et al.*, Proc. Natl. Acad. Sci. USA **116**, 12156 (2019).
[7] D. J. Scalapino, Proc. Natl. Acad. Sci. USA **116**, 12129 (2019).
[8] Q. Z. Huang and C. Q. Jin (private commmunication).
[9] K. Liu, Z.-Y. Lu, and T. Xiang, Phys. Rev. Materials **3**, 44802 (2019).
[10] T. Maier, T. Berlijn, and D. J. Scalapino, Phys. Rev. B **99**, 224515 (2019).
[11] C. Le, K. Jiang, Y. Li, S. Qin, Z. Wang, F. Zhang, and J. Hu, arXiv:1909.12620.
[12] Y. Li, S. Du, Z.-Y. Weng, and Z. Liu, Phys. Rev. Materials **4**, 044801 (2020).
[13] E. Dagotto and T. M. Rice, Science **271**, 618 (1996).
[14] F. C. Zhang, C. Gros, T. M. Rice, and H. Shiba, Supercond. Sci. Technol. **1**, 36 (1988).
[15] C. Le (private communication).
[16] F. C. Zhang and T. M. Rice, Phys. Rev. B **37**, 3759 (1988).
[17] See Supplemental Material at http://link.aps.org/supplemental/10.1103/PhysRevB.101.180509 for details of the mapping between the two lattices (Sec. I) and the details of renormalized mean-field calculations (Sec. II).
[18] S. Pathak, V. B. Shenoy, and G. Baskaran, Phys. Rev. B **81**, 085431 (2010).
[19] R. Nandkishore, L. S. Levitov, and A. V. Chubukov, Nat. Phys. **8**, 158 (2012).
[20] C. Honerkamp, Phys. Rev. Lett. **100**, 146404 (2008).
[21] W. Wu, M. M. Scherer, C. Honerkamp, and K. Le Hur, Phys. Rev. B **87**, 094521 (2013).
[22] W.-S. Wang, Y.-Y. Xiang, Q.-H. Wang, F. Wang, F. Yang, and D.-H. Lee, Phys. Rev. B **85**, 035414 (2012).
[23] M. L. Kiesel, C. Platt, W. Hanke, D. A. Abanin, and R. Thomale, Phys. Rev. B **86**, 020507(R) (2012).